The conserved protein WhiA influences branched-chain fatty acid precursors in *Bacillus subtilis*

Laura C. Bohorquez[1], Joana de Sousa[2], Transito Garcia-Garcia[3], Gaurav Dugar[1], Biwen Wang[1], Martijs J. Jonker[4], Marie-Françoise Noirot-Gros[3], Michael Lalk[2], Leendert W. Hamoen[1, #]

[1] Swammerdam Institute for Life Sciences, University of Amsterdam, Science Park 904, 1090 GE Amsterdam, The Netherlands

[2] Institute of Biochemistry, University of Greifswald, Felix-Hausdorff-Strasse 4, 17489 Greifswald, Germany

[3] Laboratoire de Genetique Microbienne, Domaine de Vilvert, Institut National de la Recherche Agronomique, 78350 Jouy-en-Josas, France

[4] RNA Biology and Applied Bioinformatics Research Group, Swammerdam Institute for Life Sciences, University of Amsterdam, Science Park 904, 1090 GE Amsterdam, The Netherlands

[#] For correspondence: L. W. Hamoen, Email: l.w.hamoen@uva.nl, Tel.: 0031-615085377

Running title: WhiA influences fatty acid composition

Keywords: WhiA, *Bacillus subtilis*, cell division, branched-chain fatty acids

ABSTRACT

The conserved WhiA protein family is present in most Gram-positive bacteria and plays a role in cell division. WhiA contains a DNA-binding motive and has been identified as a transcription factor in actinomycetes. In *Bacillus subtilis*, the absence of WhiA influences cell division and chromosome segregation, however, it is still unclear how WhiA influences these processes, but the protein does not seem to function as transcription factor in this organism. To further investigate the function of WhiA in *B. subtilis*, we performed a yeast two-hybrid screen to find interaction partners, and a Hi-C experiment to reveal possible changes in chromosome conformation. The latter experiment indicated a reduction in short range chromosome interactions, but how this would affect either cell division or chromosome segregation is unclear. Based on adjacent genes, a role in carbon metabolism was put forward. To study this, we measured exometabolome fluxes during growth on different carbon sources. This revealed that in Δ*whiA* cells the pool of branched-chain fatty acid precursors is lower. However, the effect on the membrane fatty acid composition was minimal. Transcriptome data could not link the metabolome effects to gene regulatory differences.

IMPORTANCE

WhiA is a conserved DNA binding protein that influences cell division and chromosome segregation in the Gram-positive model bacterium *B. subtilis*. The molecular function of WhiA is still unclear, but a previous study has suggested that the protein does not function as a transcription factor. In this study, we used yeast two-hybrid screening, chromosome conformation capture analysis, metabolomics, transcriptomics and fatty acid analysis to obtain

45 more information about the workings of this enigmatic protein.

INTRODUCTION

WhiA is a conserved DNA binding protein that can be found in most Gram-positive bacteria, including the simple cell wall-lacking *Mycoplasmas*. The crystal structure of *Thermotoga maritima* WhiA shows a bipartite conformation in which a degenerate N-terminal LAGLIDADG homing endonuclease domain is tethered to a C-terminal helix-turn-helix DNA binding domain. However, none of the characterized WhiA proteins have shown any nuclease activity (1). In the actinomycetes *Streptomyces*, *S. venezuelae* and *Corynebacterium glutamicum* WhiA functions as a transcriptional activator of many genes, among which the key cell division gene *ftsZ (2-4)*. Mutations in *whiA* prevent the induction of FtsZ in streptomycetes, thereby blocking synthesis of sporulation septa (5, 6). In *Bacillus subtilis,* inactivation of WhiA reduces the growth rate in rich medium and affects the expression of a variety of genes, but not that of *ftsZ* or other cell division related genes (7). Moreover, no relationship was found between WhiA binding sites on the genome and regulated genes, suggesting that WhiA does not function as a classic transcription factor in this organism (7). Nevertheless, WhiA is important for cell division in *B. subtilis*, and the absence of WhiA is synthetic lethal when cell division proteins are inactivated that regulate the formation of the Z-ring, such as the regulatory MinCD proteins, and the FtsZ polymer crosslinker ZapA (7). Later it was found that WhiA is also important for proper chromosome segregation in this organism, and *whiA* mutants display increased nucleoid spacing (8). Despite the conserved nature of this protein and its role in key cellular processes, it is unclear how this protein operates in *B. subtilis*. In the current study, we performed a wide variety of analysis, including a Yeast two-hybrid analysis, chromosome conformation capture (Hi-C), metabolomics and transcriptomics, to

68 gain a better understanding of the function of WhiA. Eventually, this led us to investigate the

69 fatty acid composition of the cell membrane in *whiA* mutants.

70

RESULTS

Yeast two-hybrid screening

To find possible interaction partners of WhiA that could help to elucidate its function, we performed a genome wide yeast two-hybrid screen (9). To increase the chances of detecting relevant interactions, we used full length WhiA, and separately its N- and C-terminal domains, containing the degenerative LAGLIDADG homing endonuclease domain (amino acids 1-227) and the helix-turn-helix domain (amino acids 222-316), respectively. The latter domain is responsible for interaction with the chromosome, which was confirmed by a microscopic analysis of GFP fusions (Fig. S1). After screening a genomic library with an approximately 15-fold redundancy of the *B. subtilis* genome, we found 3 potential interaction partners, YlxS, YrhJ and YlaD, which interacted both with full length WhiA and the N-terminal domain (Fig. S2A). Full-length WhiA showed some auto-activation in the screen. When we used the synthetic complete media lacking leucine, uracyl and adenine (-LUA), which makes the selection more stringent (9), the interaction between YlxS and full length WhiA was still observed (Fig. S2A). YlxS is 32 % identical to *Escherichia coli* RimP involved in ribosome assembly (10). YrhJ is a fatty acid monooxygenase, catalyzing hydroxylation of a range of fatty acids (11), and YlaD functions as an anti-sigma factor (12, 13). To test whether these proteins are involved in the activity of WhiA, we deleted the corresponding genes and tested for reduced growth rate in rich medium, chromosome segregation defects, and cell division phenotype in a Δ*zapA* background strain. Unfortunately, none of the deletion mutants showed a phenotype that resembled that of a Δ*whiA* mutant (Fig. S2B). It is therefore unlikely that either YlxS, YrhJ or YlaD is involved in the activity of WhiA.

Chromosome conformation

A conserved feature of Δ*whiA* mutants is the increased internucleoid distance (8). Since WhiA is a conserved DNA binding protein it might play a role in the organization of the chromosome. To examine this, we performed a Hi-C (chromosome conformation capture) analysis of Δ*whiA* cells. Both wild type and Δ*whiA* cells produced similar contact maps and the absence of WhiA does not affect the alignment of chromosome arms by the SMC condensing complex (Fig. 1A) (14). However, a clear difference was observed for short range genome interaction between the two strains (Fig. 1B). Short range interactions (< 50 kb) were reduced upon *whiA* deletion, thereby indicating potential involvement of WhiA in mediating non-specific local interaction on a genome wide scale. However, it is unclear how this would lead to increased spacing between daughter chromosomes or influence cell division.

Growth on different carbon sources

whiA is the 4th gene in an operon of 6 genes that is constitutively expressed during growth (Fig. S3) (7). The first gene, *yvcI*, encodes a Nudix hydrolase that hydrolyses organic pyrophosphates and is considered a housecleaning enzyme (15, 16). The second gene, *yvcJ,* encodes a GTPase required for the proper expression of DNA uptake proteins during natural competence (17, 18). The third gene, *yvcK*, encodes an UDP-sugar binding protein that is essential for growth under gluconeogenic conditions (19). *crH*, the fifth gene downstream of *whiA,* is a HPr-like protein that participates in catabolite repression as secondary cofactor of the global catabolite regulator CcpA (20, 21). The final gene, *yvcN*, is an uncharacterized acetyltransferase (Subtiwiki database (16)).

In many bacteria *whiA* is located adjacent to *yvcK* and *crh* (STRING database (22)). Possibly, this conserved organization points towards a metabolic function of WhiA. Inactivation of *yvcK* blocks growth on citrate and result in very poor growth on either fumarate or malate as sole carbon sources (23). To examine whether the absence of WhiA also affects growth using these carbon sources, we grew a *whiA* mutant in Spizizen minimal salt medium using either malate, fumarate or citrate as carbon source. To prevent any downstream effects, a marker-less *whiA* mutant was used, containing a stop codon at the beginning of the gene (strain KS696 (7)). As shown in Fig. 2A, the *whiA* mutant was able to grow in the different media with a growth rate similar to that of the wild-type strain, indicating that WhiA and YvcK work in different pathways. As shown in Fig. 2A and previously reported, the *whiA* mutant grows slower in rich LB medium (7). The reason that this effect was not observed in minimal medium (Fig. 2A), could be related to the lower doubling time in minimal medium compared to LB (~53 min versus ~21 min), which can mitigate chromosome segregation and cell division defects (24, 25). Therefore, we tested whether the chromosome segregation and cell division defects were present in minimal medium. Interestingly, the inter-nucleoid spacing was still larger in a *whiA* mutant (Fig. S4A), and depletion of WhiA in a Δ*zapA* background increased the cell length and occasionally generated aberrant nucleoids in minimal medium (Fig. S4B).

Utilization of carbon sources

To examine whether WhiA is involved in catabolite regulation, like *crh*, we first measured the carbon consumption by means of exometabolomics, using proton nuclear magnetic resonance spectroscopy (^{1}H-NMR) (26). This required a minimal chemically defined medium for which often

M9 medium is used. However, M9 medium has been optimized for *E. coli* and not for *B. subtilis*, and the latter easily lyses in this medium in the stationary phase (26). Therefore, we composed an alternative chemically defined medium based on different minimal media used for *B. subtilis*, as listed in Table S1. In essence, the resulting medium, named Amber medium, uses a phosphate buffer, ammonium salt and glutamate as nitrogen sources, and 22 mM for any carbon source. We tested growth on glucose alone, glucose and citrate, glucose and fumarate, and glucose and malate. Fig. 2B shows that both wild type and the marker-less *whiA* mutant grows fine in this medium using these conditions. Malate was incorporated in this analysis since it is the second preferred carbon source of *B. subtilis*, and its utilization is not subjected to carbon catabolite repression in this organism (27).

To determine the exometabolome, 2 ml of culture was collected at regular time intervals and rapidly filtered, and the filtrate stored at -20 °C for later ^{1}H-NMR spectroscopic analysis. Identification of metabolites was based on NMR spectra alignment of pure standard compounds and the quantification was done based on the integration and comparison of the designated peaks to an internal standard peak (see methods section for details). The final data were based on 3 independent biological replicates, and the quality of the replicates was confirmed using a principal component analysis (Fig. S5). As shown in Fig. 3, the consumption of the different carbon sources was the same for wild-type and *whiA* mutant cells in all 4 growth conditions. Citrate and fumarate utilization was initiated when most glucose was exhausted, confirming that fumarate and citrate were subjected to glucose-dependent catabolite repression in both strains. Malate was consumed faster than glucose as has been shown before (Meyer *et al.*, 2014). These data show that WhiA is not involved in catabolite repression.

159

160 **Exometabolome analysis**

161 Aside of the supplied carbon sources (glucose, citrate, fumarate and malate), we were able to
162 detect 18 other metabolites in the medium. Interestingly, several of these metabolites showed a
163 different secretion kinetic in the *whiA* mutant. To facilitate the interpretation of the
164 exometabolome data, the time-resolved extracellular metabolite concentrations were plotted
165 onto the relevant pathways (Fig. 4 and 5). The differences became apparent after approximately
166 180 min, when glucose levels started to go down. The depleted pools of the branched-chain fatty
167 acid precursors isovalerate, isobutyrate and 2-methylbutyrate (Fig. S7A), and the higher secretion
168 of acetate and 2-oxoglutarate in the *whiA* mutant, are most obvious. We were not able to identify
169 isoleucine, leucine and oxaloacetate due to the detection limits of the method (26). Citrate and
170 isocitrate were only measurable when the medium contained the TCA intermediate citrate or
171 fumarate (Fig. 4 lower panel, and Fig. 5 upper panel). The reason for this is that expression of
172 citrate synthase and aconitase is induced when citrate is present in the medium or fumarate
173 becomes the sole carbon source after glucose levels have fallen (26, 28).

174

175 **Transcriptome analysis**

176 To examine whether the changes in metabolism were related to changes in gene expression, we
177 compared the transcriptomes of wild type and *whiA* mutant cells grown in Amber medium
178 supplemented with glucose and malate as carbon sources. When the cultures reached an OD_{500}
179 of 0.5 (Fig. 2B, 120-180 min), cells were harvested for RNA isolation. The experiment was
180 repeated one more time to provide a biological replicate. The volcano plot in Fig. 6 depicts the

distribution of expression differences against adjusted *p*-values. 57 genes were upregulated and 40 downregulated more than 3-fold with an adjusted *p*-value < 0.05 (Table 1, data for all genes are listed in Table S7). The most highly upregulated genes, *ydcF, ydcG* and *pamR* form an operon. PamR is a transcription factor that affects expression of prophages and certain metabolic genes (29). The *bmrB* operon, coding for a multidrug ABC transporter (30), is also strongly upregulated in the *whiA* mutant. This transporter is involved in the activation of KinA, one of the key regulators of sporulation. It should be mentioned that a *whiA* mutant displays only a very mild defect in sporulation (7). The upregulated *tapA* operon is required for synthesis of the major extracellular matrix (31). Other upregulated genes were the *epeX* (*yydF*) operon encoding proteins controlling the activity of the LiaRS cell envelope stress-response system (32), the *fatR* operon involved in lipid degradation (33), and the*, sunA* and *nupN operons* necessary for biosynthesis of a siderophore, antimicrobial peptide and the uptake of guanosine, respectively *(34-36)*.

Strongly downregulated genes comprised the *wapA* operon, expressing one of the main cell surface proteins in *B. subtilis* (37), the *fadN* operon involved in fatty acid degradation (38), and the *frlB* operon coding for an amino sugar uptake system (39). Several genes involved in amino acid biosynthesis were also downregulated, including the *mtnA* operon involved in methionine salvage (40), the *tdh* operon involved in threonine utilization (41, 42), and *proHJ* necessary for production of proline (43), respectively. Finally, expression of the major citrate synthase encoded by *citZ* was also significantly downregulated (44).

The downregulation of citrate synthase did not show in the exometabolomics data, and in fact the secretion of 2-oxoglutarate, downstream of citrate in the TCA cycle, was higher in the *whiA* mutant (Fig. 5). In the medium containing citrate or fumarate as additional carbon sources,

there was also no difference in either citrate or isocitrate secretion and consumption between wild type and the mutant (Fig. 4 and 5). When we lowered the stringency and included genes that were more than 2-fold regulated (Table S7), only the 2.8-fold upregulation of *rocG*, which encodes glutamate dehydrogenase responsible for the conversion of glutamate to 2-oxoglutarate (45), could be linked to the metabolomics data, since 2-oxoglutarate levels increased faster in the *whiA* mutant in all four growth conditions (Fig. 4 and 5). However, another reason for the increased 2-oxoglutarate levels might be the reduction in branched-chain fatty acid precursors that rely on 2-oxoglutarate for the aminotransferase reaction (46). The transcriptome data did not reveal any obvious reason for the reduced synthesis of branched chain fatty acid precursors. Table S2 lists the fold-change expression of the main genes involved in branched-chain amino acids metabolism and fatty acid synthesis (see Fig. S7 for pathway schemes). The branched-chain amino acid transporters *bcaP* and *braB* were upregulated significantly by 1.9 and 1.4-fold, respectively (p-value<0.05), and so were *ybgE* and *ilvD* involved in branched-chain fatty acid precursors synthesis (1.9- and 1.5-fold, respectively). Possibly, this is a response to low substrate levels. However, *yvbW,* encoding a putative leucine permease, was downregulated 1,7-fold. The *leuA* operon involved in leucine biosynthesis was downregulated significantly but only by approximately 1.4-fold, and there was no significant difference in expression of either valine or isoleucine biosynthesis genes (Table S2). Overall, the transcriptome data did not provide a clear explanation for the exometabolome differences.

Fatty acid analysis

B. subtilis contains primarily branched-chain fatty acids. Synthesis of anteiso-fatty acids requires

isoleucine, and the iso-C15 and -C17 and iso-C14 and -C16 fatty acids require leucine and valine, respectively (de Mendoza *et al.*, 2002). Therefore, the reduced cellular concentration of these amino acids might lead to a change in the fatty acid composition of a *whiA* mutant. To investigate this, we analyzed the fatty acid composition of wild-type (strain 168) and Δ*whiA* cells (strain KS696) using gas chromatography (Table S3). For this, cells were harvested when the cultures reached an OD_{500} of approximately 0.5. The majority of fatty acids, 93.9 % in the wild type strain, are branched-chain fatty acids, and this fraction hardly changes in the Δ*whiA* mutant (93.1 %). The distribution of straight, iso and anteiso chains over the different fatty acids is shown in Fig. 7A. The fraction of iso-fatty acids in the *whiA* mutant is slightly down from 53.8 % to 45.8 %, whereas the fraction of anteiso fatty acids slightly increases from 40.1 % to 47.3 % (Fig. 7B). The reduction in leucine and valine derived fatty acids is in line with the metabolome data, but the increased contribution of isoleucine derived fatty acids is not.

Anteiso-fatty acids disturb the lipid packing more than iso-fatty acids and will therefore increase membrane fluidity, which is an important way *B. subtilis* regulates its membrane fluidity (47). This might explain why the Δ*whiA* mutant contains 2.5 % less short fatty acid species (C13, C14, C15) and 3.6 % more long fatty acid species (C16, C17, C18) (Fig. 7A), in order to maintain membrane fluidity homeostasis. Indeed, a membrane fluidity assay, using the membrane fluidity sensitive dye Laurdan (48, 49), did not detect strong differences in membrane fluidities between both strains when grown in either minimal medium or LB (not shown).

DISCUSSION

Despite the conserved nature of WhiA and its documented role as transcriptional activator in the actinomycetes, it is unclear how this protein functions in *B. subtilis*, and other Gram-positive bacteria. Hi-C data indicated that the absence of WhiA reduces short range (< 50 kb) chromosome interactions. The areas where this occurred did not correlate to WhiA binding sites that were previously determined using Chip-on-chip analysis (7). We could also not detect a clear correlation between transcription difference and the absence of these short range chromosome interactions (data not shown). However, the current resolution of the Hi-C analysis is insufficient to make such correlations. Whether the reduction in short range chromosome interactions affects chromosome segregation is unclear since there is no clear mechanism that would link these two phenomena.

Both cell division and chromosome replication are linked to the metabolic state of cells. In *B. subtilis* the glycosyltransferase UgtP couples nutritional availability to cell division (50). The protein is involved in lipoteichoic acid synthesis using UDP-glucose as substrate. Under nutrient-rich conditions, intracellular levels of UDP-glucose are high and UgtP inhibits FtsZ assembly in a UDP-glucose dependent manner. Another example is the glycolytic enzyme pyruvate dehydrogenase kinase that, by an yet unknown mechanism, positively regulates Z-ring assembly (51). Moreover, temperature sensitive mutants in the *B. subtilis* DnaC helicase, DnaG primase and DnaE polymerase can be suppressed by mutations in different glycolytic enzymes, among which pyruvate kinase (52). Since inactivation of WhiA affects both cell division and DNA segregation and since *whiA* is located in an operon adjacent to *yvcK* and *crh,* which are involved in gluconeogenic growth and catabolite repression, respectively (19, 20), it was tempting to

assume that WhiA affects cell division and chromosome replication by playing a role in carbon metabolism. However, our study showed that WhiA is neither required for gluconeogenic growth nor plays a role in carbon catabolite repression. Nevertheless, the metabolomics data did reveal that in a *whiA* mutant the pool of branched-chain fatty acid precursors is reduced. It was not possible to link this effect to changes in the transcriptome although this might be due to the fact that we measured gene regulation at the end of exponential growth, whereas the differences in the exometabolome was most apparent in the beginning of the stationary phase. Of note, several of the most strongly up- and downregulated genes were also found in a previous transcriptome study where a *whiA* deletion mutant was grown in rich LB medium, including the upregulated *ydcF, bmrB, tasA*, and *dhbE* operons, and the downregulated *mtnK* and *wapA* operons (Fig. S8) (7). However, none of these genes have so far been linked to either cell division or chromosome segregation.

Why the absence of WhiA affects branched-chain fatty acid precursor levels is unclear. It is possible that these changes have an effect on metabolic regulators that use these cofactors, such as CodY, which activity is affected by branched-chain amino acids (53). However, only a small fraction (11 %) of the CodY regulon was significantly affected in the Δ*whiA* mutant. It is also unclear how a reduction in branched-chain fatty acid precursors would influence cell division and DNA segregation in a Δ*whiA* mutant. Changes in the fatty acid composition of the membrane could in theory influence the activity of membrane proteins, however the observed differences were limited, and in fact the addition of the branched-chain fatty acid precursors isovalerate, isobutyrate and 2-methyl butyrate to LB medium did not restore the growth defect of a Δ*whiA* mutant (not shown). In conclusion, the molecular function of WhiA in *B. subtilis*, and therefore in

289 many other Gram-positive bacteria and the mycoplasmas, remains an enigma.

MATERIALS AND METHODS

Bacterial strains and growth conditions

Luria-Bertani (LB) medium was used for routine selection and maintenance of *B. subtilis* and *E. coli* strains. Spizizen's minimal medium SMM (54) consisted of 2 g/l $(NH_4)_2SO_4$, 14 g/l K_2HPO_4, 6 g/l KH_2PO_4, 1 g/l sodium citrate, 2 g/l $MgSO_4$, 5 g/l glucose, 2 g/l tryptophan, 0.2 g/l casamino acids and 2.2 g/l ammonium ferric citrate. The defined minimal (Amber) medium consisted of 70 mM K_2HPO_4 and 30 mM KH_2PO_4 (adjusted to pH 7.4), 15 mM sodium chloride, 10 mM $(NH_4)_2SO_4$, 0.002 mM of trace elements ($ZnCl_2$, $MnSO_4$, $CuCl_2$, $CoCl_2$ and Na_2MoO_4), 22 mM glucose, 0.25 mM tryptophan, 10 mM glutamate, 1 mM $MgSO_4$, 0.1 mM calcium chloride and 0.01 mM ammonium ferric citrate (Table S1). When indicated, the medium was supplemented with 22 mM final concentration of malate, fumarate or citrate. All strains were grown at 37 °C at 250 rpm. *B. subtilis* strains used in this study are listed in Table S4. The mutant strains provided by other labs were transformed into our laboratory strain to ensure isogenic backgrounds. If indicated, the medium was supplemented with a mixture of 3 branched-chain fatty acid precursors (100 µm of 2-methyl-butyrate, isobutyrate and isovalerate, Sigma-Aldrich) or straight fatty acid precursors (100 µm of methyl-butyrate, methyl-propionate and methyl-valerate, Sigma-Aldrich).

WhiA depletion strain (LB45) (8) was always grown in presence of erythromycin, due to the Campbell type integration of the P*spac-whiA* construct into the *whiA* locus. Depletion of WhiA was accomplished by inoculating a single colony into LB medium with 0.1 mM IPTG and growth at 37 °C to an OD_{600} of ~1. Subsequently, cells were harvested, washed in pre-warmed LB medium, and resuspended to an OD_{600} of 0.01 and grown in the absence of IPTG. For spot dilution

assays a single colony (strain LB45) was used to inoculate LB or Amber medium with 0.1 mM IPTG and grown at 37 °C to an OD_{600} of 0.5. Subsequently, cells were serial diluted in pre-warmed LB or Amber medium and 10 µl spots were inoculated and grown at 37 °C overnight.

Strain constructions

Molecular cloning, PCRs and transformations were carried out using standard techniques. Plasmids and oligonucleotides used in this study are listed in Table S5 and S6, respectively. The xylose inducible msfGFP-WhiA N-terminus, C-terminus and full-length fusions were constructed as follows. A PCR fragment containing *whiA* N-terminus domain, C-terminus domain and full-length were amplified with oligonucleotide pairs LB11-LB12, LB13-LB14 and LB11-LB14, respectively. Genomic DNA of strain 168 was used as template. *BamHI* and *EcoRI* restriction sites, a flexible linker and terminator were inserted into the primers. Each PCR product and the *amyE*-integration vector pHJS105 (55) were digested with *BamHI* and *EcoRI* restriction enzymes and ligated. The resulting plasmids were named pLB19, pLB20 and pLB18, respectively, verified by sequencing and transformed into *B. subtilis* 168 and competent cells, resulting in strains LB230, LB231 and LB232, respectively. Each strain was transformed with genomic DNA from *whiA* knockout KS400 (7), resulting in strains LB295, LB296 and LB294, respectively. The cellular localization of the GFP fusion proteins was determined using fluorescence microscopy.

Yeast-two hybrid assays

Proteins of interest were expressed in *Saccharomyces cerevisiae* strain PJ69-4a as fusions to the GAL4 binding domain BD or activating domain AD, from the vectors pGBDU-C1 and pGAD-C1,

334 respectively. The *whiA* N-terminal and C-terminal domains were cloned into a pGBDU bait vector
335 by gap repair and directly transformed into *S. cerevisiae* strain PJ69-4a. The DNA sequences of all
336 cloned fragments were verified by sequencing. These baits were used to screen a *B. subtilis* prey
337 library essentially as previously described (9). In brief, three *B. subtilis* genomic libraries were
338 constructed in *E. coli*, restrictions of the 4.2 Megabase *B. subtilis* chromosome produced
339 approximately 1.6 x 10^5 DNA ends that could be ligated into the pGAD prey vectors. Each library
340 contained at least 2.5 x 10^6 clones, thus providing a 15-fold redundancy. The PJ69-4a yeast strain
341 was transformed by each library DNA and at least 1.5 x 10^7 prey-containing colonies were
342 harvested and pooled. The library-containing cells were mated with bait-containing cells. The
343 mixture was plated on rich YEPD medium and incubated for 5 h at 30 °C. Cells were collected,
344 washed and spread on synthetic complete medium plates lacking the amino acids leucine and
345 histidine and the nucleotide uracil (SC-LUH). To calculate the mating efficiencies and the number
346 of diploids, cells were also spread on SC-L and SC-LU plates. A screening is covered if the number
347 of diploids is greater than 1 x 10^6 and the mating efficiency greater than 20 %. After 10-12 days
348 of incubation at 30 °C, the colonies obtained were transferred to the SC-LUA (synthetic complete
349 medium lacking leucine, uracil and adenine) and SC-LUH medium and incubated for 3-5 days. The
350 interaction candidates were identified by PCR amplification and sequencing of the DNA inserts in
351 the prey plasmids. To screen for false-positive interactions, protein-encoding prey plasmids were
352 rescued from His^+ Ade^+ colonies, reintroduced in PJ69–4alfa strain by transformation and
353 subjected to a mating with cells containing: *i*) an empty bait vector, *ii*) the initial bait used in the
354 screen and *iii*) a variety of unrelated baits. The diploid cells were tested for expression of the
355 interaction phenotypes (His^+ and Ade^+). Specific interactions were reproducible with the initial

bait and not associated with self-activation or stickiness of the prey protein. The interactions not fulfilling these criteria corresponded to false positives and were discarded.

Chromosome capture by Hi-C

Cultures were grown in LB media with shaking and samples for Hi-C were collected at exponential growth phase (OD_{600} 0.6). Hi-C was carried out exactly as described before with digestion using *HindIII* (56). Hi-C matrices were constructed using the Galaxy HiCExplorer webserver (57). Briefly, paired-end reads were mapped separately to the *B. subtilis* genome (NCBI Reference Sequence NC_000964.3) using very sensitive local setting mode in Bowtie2 (Galaxy v.2.3.4.2). The mapped files were used to build the contact matrix using the tool hicBuildMatrix (Galaxy v.2.1.2.0) using a bin size of 10 kb, and *HindIII* restriction site (AAGCTT) and AGCT as the dangling sequence. The contact matrix was then used for further analysis and visualization using the interactive browser-based visualization tool 'Bekvaem' essentially as described before (56).

Microscopy

Exponentially growing cells were stained with the fluorescent membrane dye FM-95 and the DNA was stained with DAPI. Cells were grown overnight on LB agar plates. A single colony was streaked out on LB agar plates supplemented with 0.1 % xylose for the induction of expression, grown for ~6 h and subsequently mounted on microscope slides covered with a thin film of 1 % agarose. Microscopy was performed on an inverted fluorescence Nikon Eclipse Ti microscope. The digital images were acquired and analysed with ImageJ v.1.48d5 (National Institutes of Health).

Metabolome analysis

The main culture (20 ml) was inoculated with an exponentially growing overnight culture to an initial OD_{500} of 0.05. The optical density was monitored and 2 ml cell suspension was sampled. Three experiments were carried out to provide the necessary biological replicates. During cultivation, the pH value was determined at each sampling time point by using HI 2211 pH/mV/uC bench meter (Hanna instruments Deutschland GmbH, Kehl, Germany). 2 ml of cell culture medium were taken at 60, 120, 180, 240, 300, 360, 420 and 480 min by sterile filtration, using a 0.45 mm pore size filter (Sarstedt AG, Nuernberg, Germany), to get sterile extracellular metabolite samples of the bacterial culture, and directly frozen until measurement. ^{1}H-NMR analysis was carried out as described previously (58). In brief, 400 µl of the sample was mixed with 200 µl of a sodium hydrogen phosphate buffer (0.2 M, pH 7.0) to avoid chemical shifts due to pH, which was made up with 50 % D_2O. The buffer also contained 1 mM trimethylsilyl propanoic acid-d_4 (TSP) which was used for quantification and also as a reference signal at 0.0 ppm. To obtain NMR spectra, a 1D-NOESY pulse sequence was used with a presaturation on the residual HDO signal. A total of 64 FID scans were performed with 600.27 MHz and at a temperature of 310 K using a Bruker AVANCE-II 600 NMR spectrometer operated by TOPSPIN 3.1 software (both from Bruker Biospin). For qualitative and quantitative data analysis, we used AMIX (Bruker Biospin, version 3.9.14). We used the AMIX Underground Removal Tool on obtained NMR-spectra to correct the baseline, thereby using the following parameters: left border region 20 ppm and right border region -20 ppm and a filter width of 10 Hz. Absolute quantification was performed as previously described (58). In brief, a signal of the metabolite, either a complete signal or a proportion, was chosen manually and integrated. The area was further normalized on

400 the area of the internal standard TSP and on the corresponding number of protons and the
401 sample volume. For statistical comparison of extracellular metabolite data and growth, bar-
402 charts, and XY-plots, we used Prism (version 6.01; GraphPad Software). The time-resolved
403 extracellular metabolite concentrations were $\log_2(x + 1)$ transformed for the separation via PCA.
404 The PCA was done using PAST v3.16 with auto-scaled data (59).
405
406 **Transcriptome analysis**
407 Cells (2 ml cultures) were spun down (30 s Eppendorf centrifuge, 14,000 rpm, 4 °C), resuspended
408 in 0.4 ml ice-cold growth medium and added to a screw cap Eppendorf tube containing 1.5 g glass
409 beads (0.1 mm), 500 µl phenol:chloroform:isoamyl alcohol (25:24:1), 50 µl 10 % SDS and 50 µl
410 RNAse free water (60). All solutions were prepared with diethylpyrocarbonate (DEPC)-treated
411 water. After vortexing, tubes were frozen in liquid nitrogen and stored at -80 °C. Cells were
412 broken using a bead-beater for 4 min at room temperature. After centrifugation, the water phase
413 was transferred to a clean tube containing 400 µl chloroform, after vortexing and centrifugation,
414 the water phase was used for RNA isolation with High Pure RNA Isolation Kit (Roche Diagnostics
415 GmbH, Mannheim, Germany), yielding >3 µg total RNA per sample. TapeStation System (Agilent)
416 was used for checking the integrity of the RNA, and RIN values of 8.3 – 9.2 were obtained. For
417 next-generation sequencing, a ribosomal RNA depletion was performed on the total RNA using
418 the Ribo-Zero rRNA Removal Kit (Gram-Positive Bacteria) (Illumina). Bar-coded RNA libraries
419 were generated according to the manufacturers' protocols using the Ion Total RNA-Seq Kit v2
420 and the Ion Xpress RNA-Seq barcoding kit (Thermo Fisher Scientific). The size distribution and
421 yield of the barcoded libraries were assessed using the 2200 TapeStation System with Agilent

D1000 ScreenTapes (Agilent Technologies). Sequencing templates were prepared on the Ion Chef System using the Ion PI Hi-Q Chef Kit (Thermo Fisher Scientific). Sequencing was performed on an Ion Proton System using an Ion PI v3 chip (Thermo Fisher Scientific) according to the instructions of the manufacturer. After quality control and trimming the sequence reads were mapped onto the genome (genome-build-accession NCBI Assembly: GCA_000009045.1) using the Torrent Mapping Alignment Program. The Ion Proton system generates sequence reads of variable lengths, and this program combines a short read algorithm (61), and long read algorithms (62) in a multistage mapping approach. The gene expression levels were quantified using HTseq (63). The data was normalized and analysed for differential expression using R statistical software and the DESeq2 package (64). The RNA-seq data have been submitted to and are accessible in the Gene Expression Omnibus (GEO) using accession number GSE121479.

Lipid analysis

The fatty acid composition was determined from cells growing in Amber medium when the cultures reached an OD_{600} of approximately 0.5. Cells were harvest by centrifugation at 10.000x rcf for 5 min at 4 °C, washed once with 0.9 % ice-cold NaCl, and submitted to flash freeze in liquid N_2. Fatty acids were analyzed as fatty acid methyl esters (FAME) using gas chromatography. All analyses were carried out in triplicates at theLaboratory Genetic Metabolic Disease, Amsterdam UMC .

Laurdan GP spectroscopy

For the measurement of membrane fluidity in batch cultures as reported before (49), cells were

grown in either LB or Spizizen minimal salt medium (SMM) to an OD of approximately 0.5, followed by 5 min incubation with 10 mM Laurdan. Subsequently, cells were washed three times with pre-warmed buffer containing 50 mM Na_2HPO_4/NaH_2PO_4 pH 7.4, 0.1 % glucose and 150 mM NaCl with and without the membrane fluidizer benzyl alcohol (30 mM). The Laurdan fluorescence intensities were measured at 435±5 nm and 490±5 nm upon excitation at 350±10 nm, using a Tecan Infinite 200M fluorometer. The Laurdan generalized polarization (GP) was calculated using the formula $GP = (I_{435} - I_{490}) / (I_{435} + I_{490})$.

ACKNOWLEDGEMENTS

We would like to thank Henrik Strahl (Newcastle University) for scientific assistance with the lipid analysis and for insightful discussions, Johan Westerhuis (University of Amsterdam) for his insights about the analysis of the exometabolome, Selina van Leeuwen (MAD, UvA) for providing excellent sequencing services, and to all the members of the Bacterial Cell Biology group (University of Amsterdam), and specially to all the members of the Advanced Multidisciplinary Training in Molecular Bacteriology (AMBER) EU Marie Curie Initial Training Network (ITN). The research was funded by EU Marie Curie ITN grant AMBER (317338), Marie Curie CIG grant DIVANTI (618452), European Commission MCSA-IF 749510, and STW Vici grant 12128.

REFERENCES

1. Kaiser BK, Clifton MC, Shen BW, Stoddard BL. 2009. The structure of a bacterial DUF199/WhiA protein: domestication of an invasive endonuclease. Structure 17:1368-76.
2. Bush MJ, Bibb MJ, Chandra G, Findlay KC, Buttner MJ. 2013. Genes required for aerial growth, cell division, and chromosome segregation are targets of WhiA before sporulation in *Streptomyces venezuelae*. mBio 4:e00684-13.
3. Lee DS, Kim P, Kim ES, Kim Y, Lee HS. 2018. *Corynebacterium glutamicum* WhcD interacts with WhiA to exert a regulatory effect on cell division genes. Antonie Van Leeuwenhoek 111:641-648.
4. McCormick JR, Flardh K. 2012. Signals and regulators that govern Streptomyces development. FEMS Microbiol Rev 36:206-31.
5. Ainsa JA, Ryding NJ, Hartley N, Findlay KC, Bruton CJ, Chater KF. 2000. WhiA, a protein of unknown function conserved among gram-positive bacteria, is essential for sporulation in *Streptomyces coelicolor* A3(2). J Bacteriol 182:5470-8.
6. Flardh K, Leibovitz E, Buttner MJ, Chater KF. 2000. Generation of a non-sporulating strain of *Streptomyces coelicolor* A3(2) by the manipulation of a developmentally controlled *ftsZ* promoter. Mol Microbiol 38:737-49.
7. Surdova K, Gamba P, Claessen D, Siersma T, Jonker MJ, Errington J, Hamoen LW. 2013. The conserved DNA-binding protein WhiA is involved in cell division in *Bacillus subtilis*. J Bacteriol 195:5450-60.
8. Bohorquez LC, Surdova K, Jonker MJ, Hamoen LW. 2018. The Conserved DNA Binding Protein WhiA Influences Chromosome Segregation in *Bacillus subtilis*. J Bacteriol 200.
9. Noirot-Gros MF, Dervyn E, Wu LJ, Mervelet P, Errington J, Ehrlich SD, Noirot P. 2002. An expanded view of bacterial DNA replication. Proc Natl Acad Sci U S A 99:8342-7.
10. Nord S, Bylund GO, Lovgren JM, Wikstrom PM. 2009. The RimP protein is important for maturation of the 30S ribosomal subunit. J Mol Biol 386:742-53.
11. Lentz O, Urlacher V, Schmid RD. 2004. Substrate specificity of native and mutated cytochrome P450 (CYP102A3) from *Bacillus subtilis*. J Biotechnol 108:41-9.
12. Matsumoto T, Nakanishi K, Asai K, Sadaie Y. 2005. Transcriptional analysis of the *ylaABCD* operon of *Bacillus subtilis* encoding a sigma factor of extracytoplasmic function family. Genes Genet Syst 80:385-93.
13. Ryu HB, Shin I, Yim HS, Kang SO. 2006. YlaC is an extracytoplasmic function (ECF) sigma factor contributing to hydrogen peroxide resistance in *Bacillus subtilis*. J Microbiol 44:206-16.
14. Wang X, Le TB, Lajoie BR, Dekker J, Laub MT, Rudner DZ. 2015. Condensin promotes the juxtaposition of DNA flanking its loading site in *Bacillus subtilis*. Genes Dev 29:1661-75.
15. Mildvan AS, Xia Z, Azurmendi HF, Saraswat V, Legler PM, Massiah MA, Gabelli SB, Bianchet MA, Kang LW, Amzel LM. 2005. Structures and mechanisms of Nudix hydrolases. Arch Biochem Biophys 433:129-43.
16. Michna RH, Zhu B, Mader U, Stulke J. 2016. SubtiWiki 2.0 - an integrated database for the model organism *Bacillus subtilis*. Nucleic Acids Res 44:D654-62.
17. Luciano J, Foulquier E, Fantino JR, Galinier A, Pompeo F. 2009. Characterization of YvcJ, a conserved P-loop-containing protein, and its implication in competence in *Bacillus subtilis*. J Bacteriol 191:1556-64.

18. Pompeo F, Luciano J, Brochier-Armanet C, Galinier A. 2011. The GTPase function of YvcJ and its subcellular relocalization are dependent on growth conditions in *Bacillus subtilis*. J Mol Microbiol Biotechnol 20:156-67.
19. Gorke B, Foulquier E, Galinier A. 2005. YvcK of *Bacillus subtilis* is required for a normal cell shape and for growth on Krebs cycle intermediates and substrates of the pentose phosphate pathway. Microbiology 151:3777-91.
20. Galinier A, Haiech J, Kilhoffer MC, Jaquinod M, Stulke J, Deutscher J, Martin-Verstraete I. 1997. The *Bacillus subtilis crh* gene encodes a HPr-like protein involved in carbon catabolite repression. Proc Natl Acad Sci USA 94:8439-44.
21. Landmann JJ, Busse RA, Latz JH, Singh KD, Stulke J, Gorke B. 2011. Crh, the paralogue of the phosphocarrier protein HPr, controls the methylglyoxal bypass of glycolysis in *Bacillus subtilis*. Mol Microbiol 82:770-87.
22. Szklarczyk D, Gable AL, Lyon D, Junge A, Wyder S, Huerta-Cepas J, Simonovic M, Doncheva NT, Morris JH, Bork P, Jensen LJ, Mering CV. 2019. STRING v11: protein-protein association networks with increased coverage, supporting functional discovery in genome-wide experimental datasets. Nucleic Acids Res 47:D607-D613.
23. Foulquier E, Pompeo F, Bernadac A, Espinosa L, Galinier A. 2011. The YvcK protein is required for morphogenesis via localization of PBP1 under gluconeogenic growth conditions in *Bacillus subtilis*. Mol Microbiol 80:309-18.
24. Arjes HA, Kriel A, Sorto NA, Shaw JT, Wang JD, Levin PA. 2014. Failsafe mechanisms couple division and DNA replication in bacteria. Curr Biol 24:2149-2155.
25. Galli E, Midonet C, Paly E, Barre FX. 2017. Fast growth conditions uncouple the final stages of chromosome segregation and cell division in *Escherichia coli*. PLoS Genet 13:e1006702.
26. Meyer H, Weidmann H, Mader U, Hecker M, Volker U, Lalk M. 2014. A time resolved metabolomics study: the influence of different carbon sources during growth and starvation of *Bacillus subtilis*. Mol Biosyst 10:1812-23.
27. Doan T, Servant P, Tojo S, Yamaguchi H, Lerondel G, Yoshida KI, Fujita Y, Aymerich S. 2003. The *Bacillus subtilis ywkA* gene encodes a malic enzyme and its transcription is activated by the YufL/YufM two-component system in response to malate. Microbiology (Reading) 149:2331-2343.
28. Sonenshein AL. 2007. Control of key metabolic intersections in *Bacillus subtilis*. Nat Rev Microbiol 5:917-27.
29. De San Eustaquio-Campillo A, Cornilleau C, Guerin C, Carballido-Lopez R, Chastanet A. 2017. PamR, a new MarR-like regulator affecting prophages and metabolic genes expression in *Bacillus subtilis*. PLoS One 12:e0189694.
30. Torres C, Galian C, Freiberg C, Fantino JR, Jault JM. 2009. The YheI/YheH heterodimer from *Bacillus subtilis* is a multidrug ABC transporter. Biochim Biophys Acta 1788:615-22.
31. Branda SS, Gonzalez-Pastor JE, Ben-Yehuda S, Losick R, Kolter R. 2001. Fruiting body formation by *Bacillus subtilis*. Proc Natl Acad Sci U S A 98:11621-6.
32. Butcher BG, Lin YP, Helmann JD. 2007. The *yydFGHIJ* operon of *Bacillus subtilis* encodes a peptide that induces the LiaRS two-component system. J Bacteriol 189:8616-25.
33. Palmer CN, Gustafsson MC, Dobson H, von Wachenfeldt C, Wolf CR. 1999. Adaptive responses to fatty acids are mediated by the regulated expression of cytochromes P450. Biochem Soc Trans 27:374-8.

549 34. May JJ, Wendrich TM, Marahiel MA. 2001. The *dhb* operon of *Bacillus subtilis* encodes the
550 biosynthetic template for the catecholic siderophore 2,3-dihydroxybenzoate-glycine-
551 threonine trimeric ester bacillibactin. J Biol Chem 276:7209-17.
552 35. Paik SH, Chakicherla A, Hansen JN. 1998. Identification and characterization of the structural
553 and transporter genes for, and the chemical and biological properties of, sublancin 168, a
554 novel lantibiotic produced by *Bacillus subtilis* 168. J Biol Chem 273:23134-42.
555 36. Molle V, Nakaura Y, Shivers RP, Yamaguchi H, Losick R, Fujita Y, Sonenshein AL. 2003.
556 Additional targets of the *Bacillus subtilis* global regulator CodY identified by chromatin
557 immunoprecipitation and genome-wide transcript analysis. J Bacteriol 185:1911-22.
558 37. Koskiniemi S, Lamoureux JG, Nikolakakis KC, t'Kint de Roodenbeke C, Kaplan MD, Low DA,
559 Hayes CS. 2013. Rhs proteins from diverse bacteria mediate intercellular competition. Proc
560 Natl Acad Sci U S A 110:7032-7.
561 38. Matsuoka H, Hirooka K, Fujita Y. 2007. Organization and function of the YsiA regulon of
562 *Bacillus subtilis* involved in fatty acid degradation. J Biol Chem 282:5180-94.
563 39. Deppe VM, Klatte S, Bongaerts J, Maurer KH, O'Connell T, Meinhardt F. 2011. Genetic control
564 of amadori product degradation in *Bacillus subtilis* via regulation of *frlBONMD* expression by
565 FrlR. Appl Environ Microbiol 77:2839-46.
566 40. Sekowska A, Mulard L, Krogh S, Tse JK, Danchin A. 2001. MtnK, methylthioribose kinase, is a
567 starvation-induced protein in *Bacillus subtilis*. BMC Microbiol 1:15.
568 41. Zhang L, Cao Y, Tong J, Xu Y. 2019. An Alkylpyrazine Synthesis Mechanism Involving l-
569 Threonine-3-Dehydrogenase Describes the Production of 2,5-Dimethylpyrazine and 2,3,5-
570 Trimethylpyrazine by *Bacillus subtilis*. Appl Environ Microbiol 85.
571 42. Plata G, Fuhrer T, Hsiao TL, Sauer U, Vitkup D. 2012. Global probabilistic annotation of
572 metabolic networks enables enzyme discovery. Nat Chem Biol 8:848-54.
573 43. Belitsky BR, Brill J, Bremer E, Sonenshein AL. 2001. Multiple genes for the last step of proline
574 biosynthesis in *Bacillus subtilis*. J Bacteriol 183:4389-92.
575 44. Jin S, Sonenshein AL. 1994. Identification of two distinct *Bacillus subtilis* citrate synthase
576 genes. J Bacteriol 176:4669-79.
577 45. Commichau FM, Wacker I, Schleider J, Blencke HM, Reif I, Tripal P, Stulke J. 2007.
578 Characterization of *Bacillus subtilis* mutants with carbon source-independent glutamate
579 biosynthesis. J Mol Microbiol Biotechnol 12:106-13.
580 46. Berger BJ, English S, Chan G, Knodel MH. 2003. Methionine regeneration and
581 aminotransferases in *Bacillus subtilis*, *Bacillus cereus*, and *Bacillus anthracis*. J Bacteriol
582 185:2418-31.
583 47. Diomande SE, Nguyen-The C, Guinebretiere MH, Broussolle V, Brillard J. 2015. Role of fatty
584 acids in Bacillus environmental adaptation. Front Microbiol 6:813.
585 48. Parasassi T, De Stasio G, d'Ubaldo A, Gratton E. 1990. Phase fluctuation in phospholipid
586 membranes revealed by Laurdan fluorescence. Biophys J 57:1179-86.
587 49. Strahl H, Burmann F, Hamoen LW. 2014. The actin homologue MreB organizes the bacterial
588 cell membrane. Nat Commun 5:3442.
589 50. Weart RB, Lee AH, Chien AC, Haeusser DP, Hill NS, Levin PA. 2007. A metabolic sensor
590 governing cell size in bacteria. Cell 130:335-47.
591 51. Monahan LG, Hajduk IV, Blaber SP, Charles IG, Harry EJ. 2014. Coordinating bacterial cell
592 division with nutrient availability: a role for glycolysis. mBio 5:e00935-14.

593 52. Janniere L, Canceill D, Suski C, Kanga S, Dalmais B, Lestini R, Monnier AF, Chapuis J, Bolotin
594 A, Titok M, Le Chatelier E, Ehrlich SD. 2007. Genetic evidence for a link between glycolysis
595 and DNA replication. PLoS One 2:e447.
596 53. Shivers RP, Sonenshein AL. 2004. Activation of the *Bacillus subtilis* global regulator CodY by
597 direct interaction with branched-chain amino acids. Mol Microbiol 53:599-611.
598 54. Spizizen J. 1958. Transformation of biochemically deficient strains of *Bacillus subtilis* by
599 deoxyribonucleate. Proc Natl Acad Sci U S A 44:1072-8.
600 55. Jahn N, Brantl S, Strahl H. 2015. Against the mainstream: the membrane-associated type I
601 toxin BsrG from *Bacillus subtilis* interferes with cell envelope biosynthesis without increasing
602 membrane permeability. Mol Microbiol 98:651-66.
603 56. Dugar G, Hofmann A, Heermann DW, Hamoen LW. 2022. A chromosomal loop anchor
604 mediates bacterial genome organization. Nat Genet 54:194-201.
605 57. Wolff J, Bhardwaj V, Nothjunge S, Richard G, Renschler G, Gilsbach R, Manke T, Backofen R,
606 Ramirez F, Gruning BA. 2018. Galaxy HiCExplorer: a web server for reproducible Hi-C data
607 analysis, quality control and visualization. Nucleic Acids Res 46:W11-W16.
608 58. Dorries K, Lalk M. 2013. Metabolic footprint analysis uncovers strain specific overflow
609 metabolism and D-isoleucine production of *Staphylococcus aureus* COL and HG001. PLoS
610 One 8:e81500.
611 59. van den Berg RA, Hoefsloot HC, Westerhuis JA, Smilde AK, van der Werf MJ. 2006. Centering,
612 scaling, and transformations: improving the biological information content of metabolomics
613 data. BMC Genomics 7:142.
614 60. Hamoen LW, Smits WK, de Jong A, Holsappel S, Kuipers OP. 2002. Improving the predictive
615 value of the competence transcription factor (ComK) binding site in *Bacillus subtilis* using a
616 genomic approach. Nucleic Acids Res 30:5517-28.
617 61. Li H, Durbin R. 2009. Fast and accurate short read alignment with Burrows-Wheeler
618 transform. Bioinformatics 25:1754-60.
619 62. Li H, Durbin R. 2010. Fast and accurate long-read alignment with Burrows-Wheeler
620 transform. Bioinformatics 26:589-95.
621 63. Anders S, Pyl PT, Huber W. 2015. HTSeq--a Python framework to work with high-throughput
622 sequencing data. Bioinformatics 31:166-9.
623 64. Love MI, Huber W, Anders S. 2014. Moderated estimation of fold change and dispersion for
624 RNA-seq data with DESeq2. Genome Biol 15:550.
625

626 **Table 1.** Transcriptome comparison of wild-type (strain 168) and *whiA* marker-less mutant cells
627 (strain KS696). Cells were grown in defined minimal (Amber) medium with glucose and malate
628 and harvested for RNA isolation during exponential growth (OD_{600} ~0.5). Genes with an adjusted
629 *p*-value < 0.05 and Fold Change (FC) > 3 (Δ*whiA*/wt) are listed. Genes found in a previous
630 transcriptome Δ*whiA* analysis performed in LB rich medium are indicated by * (7) (see also Fig.
631 S8). Genes located in one operon are listed together in one row.

Gene	FC	Function
Upregulated		
ydcF-G*- pamR**	24-50	unknown
bmrB-C-D**	4-14	multidrug ABC transporter
tapA-sipW*-tasA**	4-6	major component of biofilm matrix
yxbB-A-yxnB-asnH-yxaM	3-5	biosynthesis of asparagine & unknown
yxbC-D	3	unknown (upstream of yxbB operon)
yrzI	5,1	unknown
epeX-E-P-A-B	2-5	control of LiaRS cell envelope stress system
ybdZ	3.4	unknown
yfmG	3.2	unknown
fatR-yrhJ	3	fatty acid metabolism
dhbA-C*-E*-B*-F**	3	biosynthesis of the siderophore bacillibactin
*besA**	2.4	iron acquisition, ferri-bacillibactin esterase
yobB	3.5	unknown
sunA-T-bdbA-sunA-bdbB*	3-4	sublancin lantibiotic production & thiol-disulfide oxidoreductase
yitP-O-M	3	biofilm toxin & unknown
nupN-O-P	3	uptake of guanosine
yoaW	3.1	secreted protein with unknown function
ybdN	3.1	unknown
yyzI	3.1	unknown
skfA-B-C-E-F-G-H	2-4	spore killing factor
Downregulated		
mtnU-A*-K**	-(3-6)	methionine salvage
wapA-I*-yxzC*-G*-J*-I*-yxiG*-H*-I*-J*-K*-M**	-5.9	cell wall-associated WapA protein toxin & unknown
yonN-J-B-yomW-U-Z	-(3-4)	parts of SP-beta prophage genome
fadN-A-E	-4	fatty acid degradation
bsdB-C-yclD	-(3-4)	resistance to salicylic acid
Tdh-kbl	-(3-4)	threonine utilization
frlB-O-N-M	-(3-4)	fructose metabolism
yezD	-3.4	unknown
proH-J	-3	osmoadaptive de novo production of proline
oxdC	-3.2	oxalate decarboxylase
licH	-3.0	6-phospho-beta-glucosidase, lichenan utilization
citZ	-3.0	citrate synthase, TCA cycle

632

633 **Figure 1**

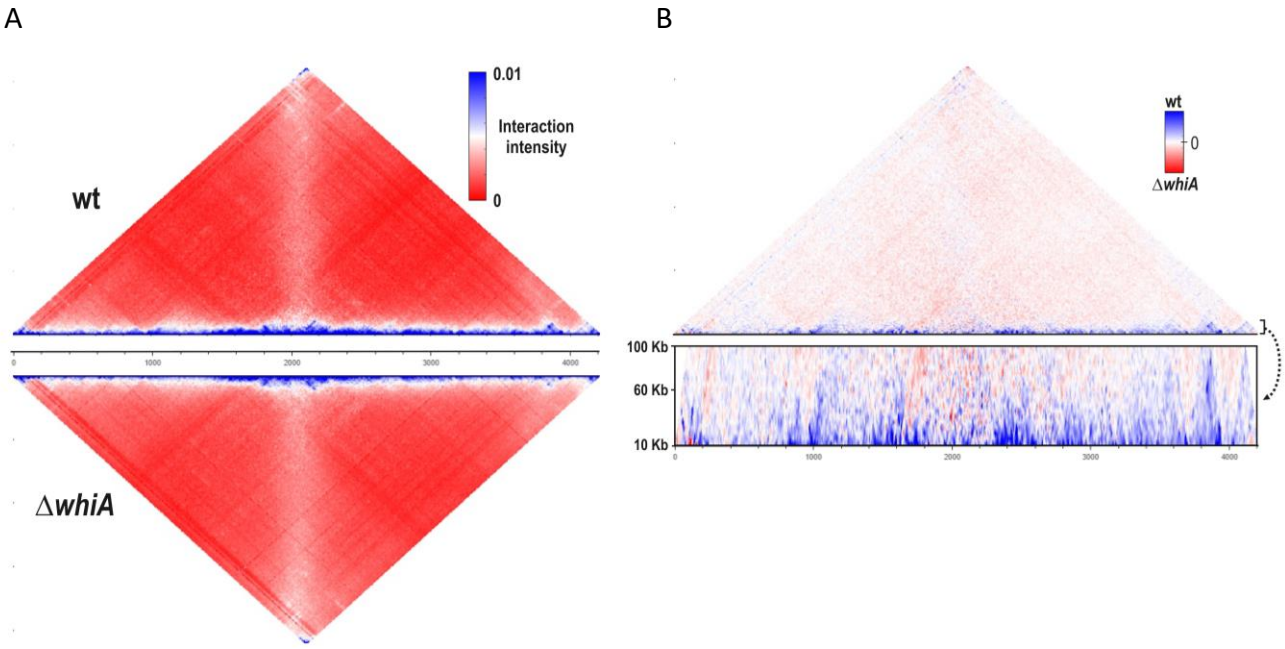

634

635

636 **Fig. 1. Chromosome conformation capture (Hi-C) analysis.**

637 (A) Normalized Hi-C contact maps of wild type (top) and Δ*whiA* strains (below) at exponential

638 phase. SMC dependent juxtaposition of the chromosome arms is observed in both strains as the

639 secondary (vertical) diagonal (14). (B) Difference plot of wild type and Δ*whiA* strains. The

640 magnified view of difference in short-range contacts (between 10 kb and 100 kb) is shown below.

641 **Figure 2**

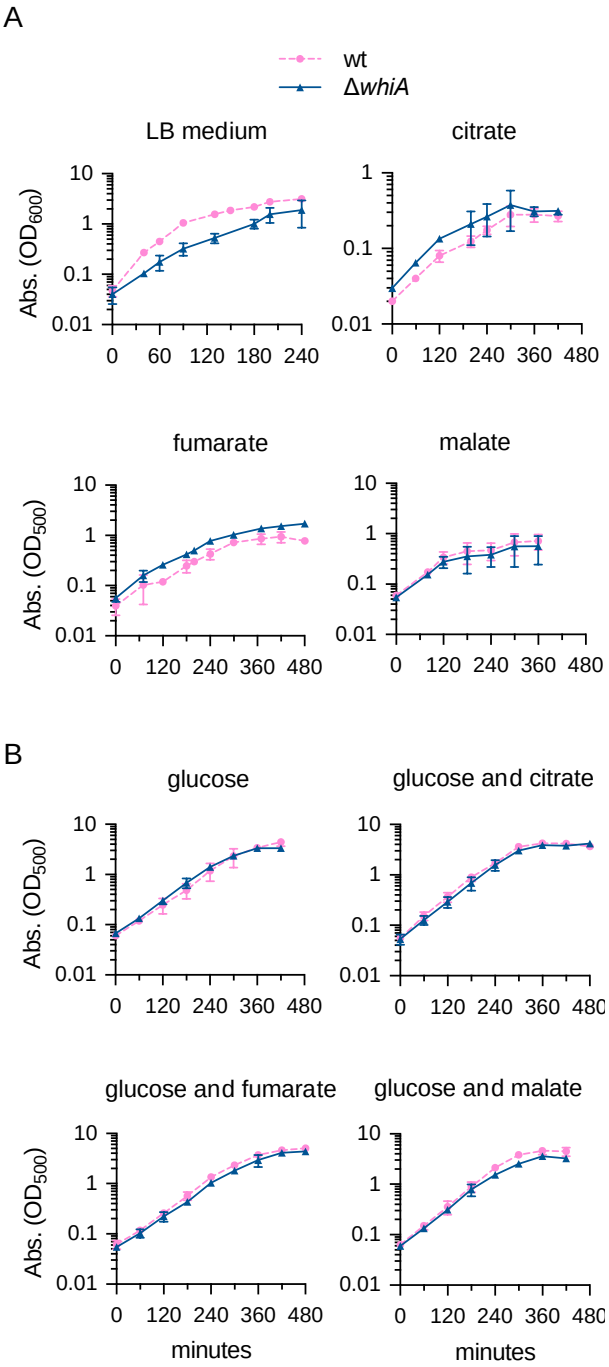

642

643 **Fig. 2. Growth on different carbon sources.**

644 Growth measured as optical density of the wild-type strain (strain 168) and the *whiA* marker-less

645 mutant (strain KS696). (A) Growth in LB medium, and in Spizizen minimal salt medium (SMM)

646 supplemented with 22 mM of either citrate, fumarate or malate. (B) Growth in chemically defined
647 minimal Amber medium supplemented with 22 mM of either glucose, glucose and citrate,
648 glucose and fumarate or glucose and malate. Data are shown as mean values and standard
649 deviation of triplicate samples.

650

651

652 **Figure 3**

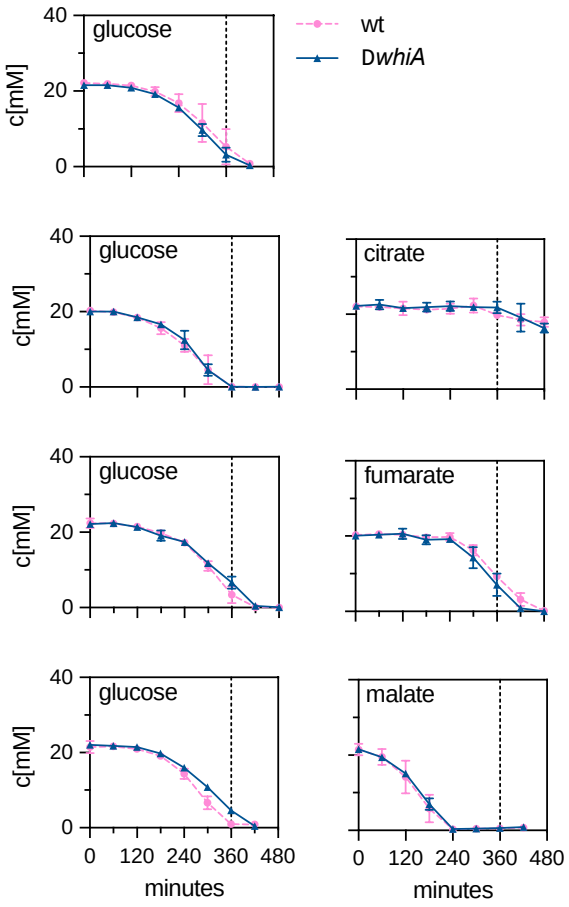

653

654 **Fig. 3. Carbon utilization.**

655 Carbon source utilization (concentration in mM) of wild-type (strain 168) and *whiA* marker-less
656 mutant cells (strain KS696) during growth in defined minimal (Amber) medium supplemented
657 with either glucose, glucose and malate, glucose and citrate or glucose and fumarate (22 mM
658 each). Data are shown as mean values and standard deviation of triplicate samples. The dashed
659 lines mark the time point when the glucose culture enters stationary phase (360 min) (see Fig.
660 2B).

661

662 **Figure 4**

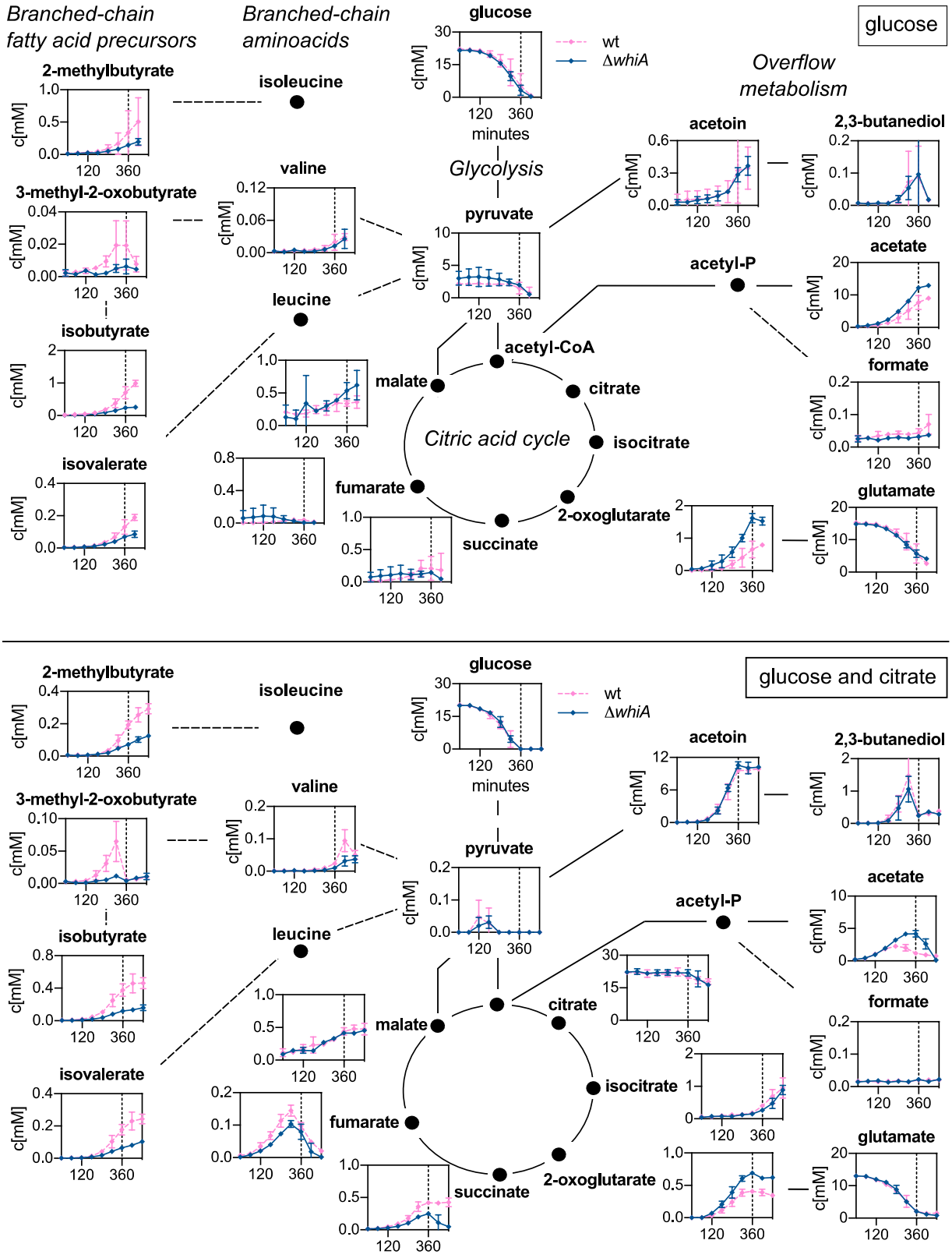

663

664 **Fig. 4. Exometabolome of cells grown with either glucose or glucose and citrate.**

665 Time-resolved extracellular metabolite concentrations (in mM) of wild-type (strain 168) and *whiA*
666 marker-less mutant cells (strain KS696) grown in chemically defined minimal Amber medium with
667 either glucose alone (upper panel) or glucose and citrate (lower panel) as carbon source (22 mM
668 each). Dashed lines indicate entry into stationary phase (360 min). The compounds are arranged
669 according to the main metabolic pathways: glycolysis, TCA cycle, overflow metabolites,
670 branched-chain amino acids and branched-chain fatty acids precursors. Data are shown as mean
671 values and standard deviation of triplicate samples.
672

673 **Figure 5**

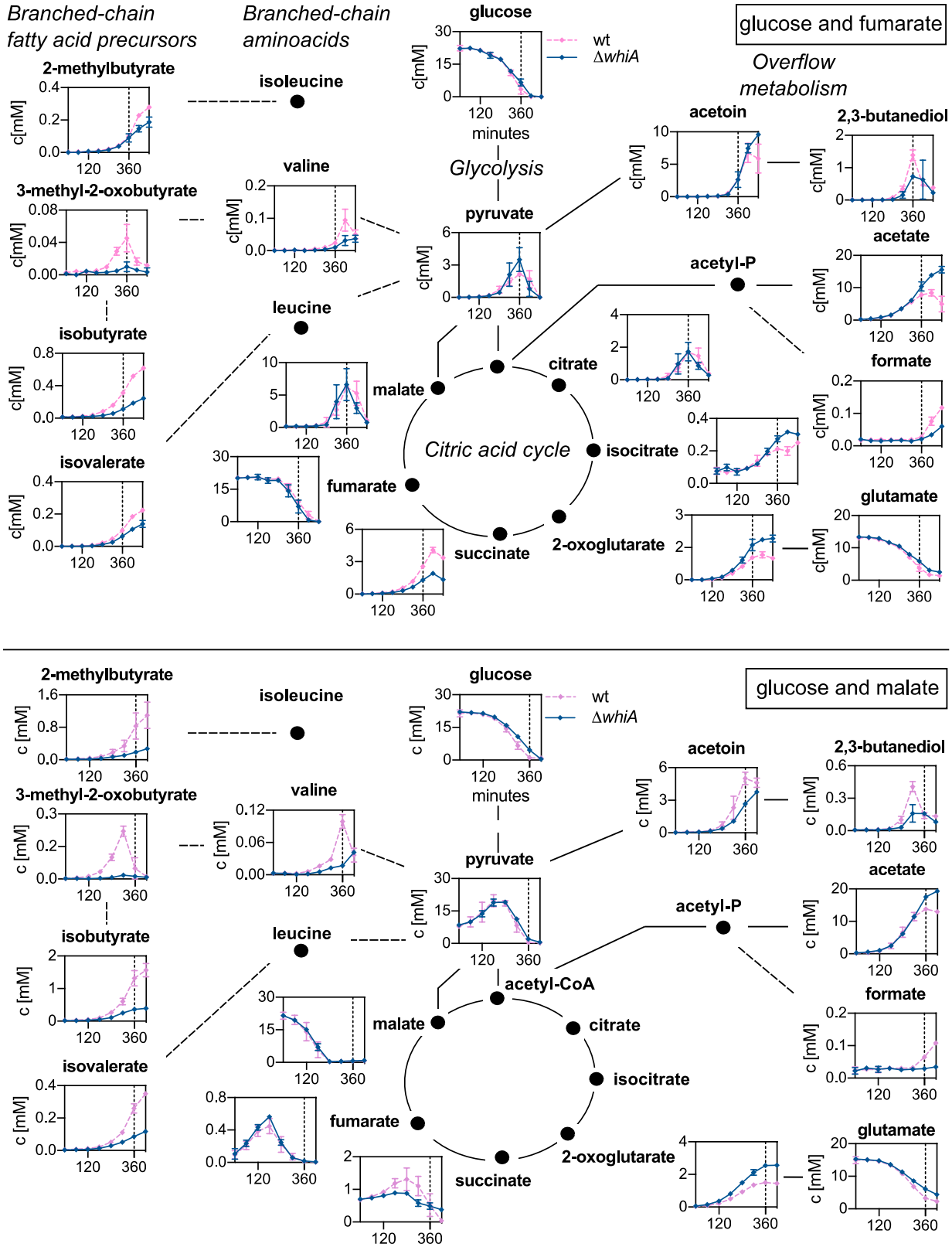

674 **Fig. 5. Exometabolome in cells grown with either glucose and fumarate or glucose and malate.**
675 Time-resolved extracellular metabolite concentrations (in mM) of wild-type (strain 168) and *whiA*
676 marker-less mutant cells (strain KS696) grown in chemically defined minimal Amber medium with
677 either glucose and fumarate (upper panel) or glucose and malate (lower panel) as carbon sources
678 (22 mM each). Dashed lines indicate entry into stationary phase (360 min). The compounds are
679 arranged according to the main metabolic pathways: glycolysis, TCA cycle, overflow metabolites,
680 branched-chain amino acids and branched-chain fatty acids precursors. Data are shown as mean
681 values and standard deviation of triplicate samples.
682

683 **Figure 6**

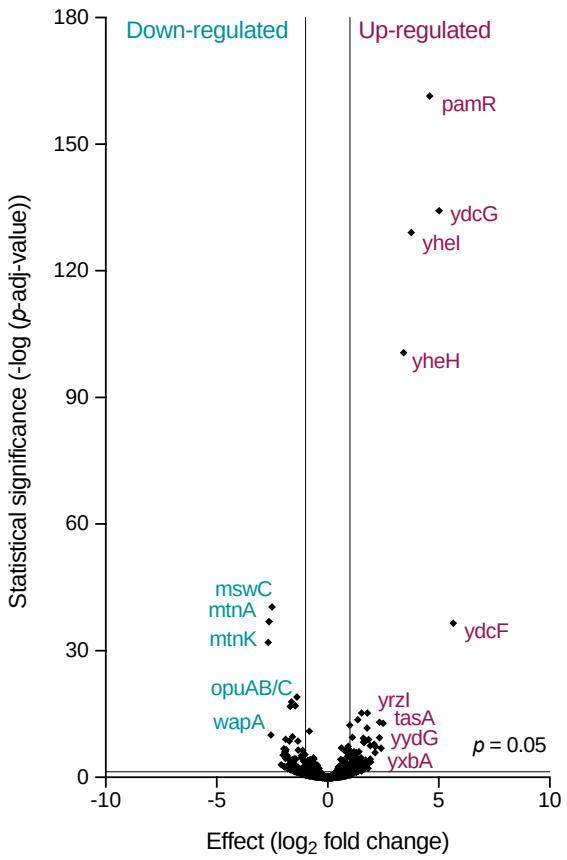

684

685 **Fig. 6. Volcano plot of transcriptome data**

686 Volcano plot depicting the transcriptome data as a relation between adjusted *p*-values and $\log_2$

687 fold expression change. Wild-type (strain 168) and *whiA* marker-less mutant cells (strain KS696)

688 were grown in defined minimal (Amber) medium with glucose and malate and sampled during

689 exponential growth. Main downregulated and upregulated genes in the *whiA* mutant are shown

690 in green and red, respectively. Genes are listed in Table S2.

691

692

693 **Figure 7**

694

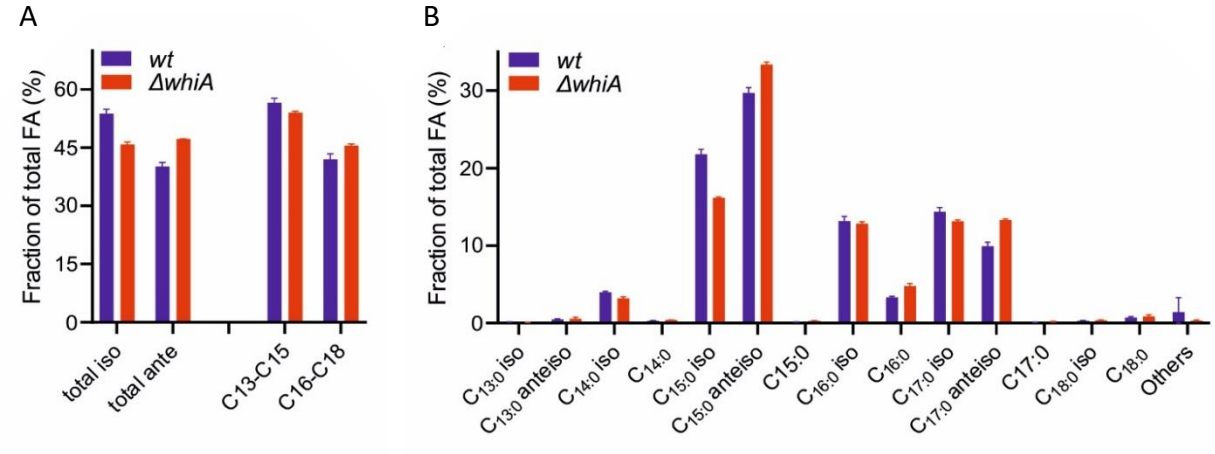

695

696 **Fig. 7. Fatty acid analysis of Δ*whiA* mutant.**

697 (A) Comparison of the total iso- and anteiso-fatty acids and fatty acid chain length between wild

698 type *B. subtilis* and Δ*whiA* cells. (B) Detailed comparison of the different fatty acids.

699 Concentrations of individual fatty acids are listed in Table S3.

700